Molybdenum isotopes in plume-influenced MORBs reveal recycling of ancient anoxic sediments

Q. Ahmad, M. Wille, C. Rosca, Jabrane Labidi, T. Schmid, K. Mezger, S. König

Molybdenum isotopes in plume-influenced MORBs reveal recycling of ancient anoxic sediments

Qasid **Ahmad**[1*] (qasid.ahmad@geo.unibe.ch)
Martin **Wille**[1] (martin.wille@geo.unibe.ch)
Carolina **Rosca**[2] (carolina.rosca@uni-tuebingen.de)
Jabrane **Labidi**[3] (labidi@ipgp.fr)
Timothy **Schmid**[1] (timothy.schmid@geo.unibe.ch)
Klaus **Mezger**[1,4] (klaus.mezger@geo.unibe.ch)
Stephan **König**[5] (s.konig@csic.es)

[1]Institut für Geologie, Universität Bern, Baltzerstrasse 1+3, 3012 Bern, Switzerland
[2]Fachbereich Geowissenschaften – Isotopengeochemie, Geo- und Umweltforschungszentrum, Eberhard Karls Universität Tübingen, Schnarrenbergstrasse 94-96, 72076 Tübingen, Germany
[3]Université de Paris, Institut de physique du globe de Paris, CNRS, Paris, France
[4]Center for Space and Habitability, Universität Bern, Gesellschaftsstrasse 6, 3012 Bern, Switzerland
[5]Instituto Andaluz de Ciencias de la Tierra (IACT), CSIC & UGR, Avenida las Palmeras 4, Armilla, 18100 Granada, Spain

Submitted to: Geochemical Perspectives Letters

Keywords: Molybdenum isotopes, subduction zones, MORB, sediments, mantle-plume, redox

Corresponding author:
Qasid Ahmad
(qasid.ahmad@geo.unibe.ch)

Abstract

Under modern oxidising Earth surface conditions, dehydrated subducted slabs show Mo isotope compositions as low as $\delta^{98/95}$Mo = -1.5 ‰, compared to the depleted mantle $\delta^{98/95}$Mo = -0.2 ‰. Such light Mo isotope compositions reflect the redox-dependent aqueous mobility of isotopically heavy Mo associated with slab dehydration. Here we analysed basaltic glasses from the South-Mid Atlantic Ridge, whose parental melts are influenced by the enriched Discovery and Shona mantle-plumes. We report increasingly higher $\delta^{98/95}$Mo of up to -0.1 ‰ from the most depleted samples towards those tapping more enriched mantle sources. $\delta^{98/95}$Mo values correlate positively with radiogenic Sr and Nd isotopes, which indicates recycling of Proterozoic sediments with a Mo isotopic composition that was not affected by subduction-related, oxic dehydration. We propose that the Mo isotope signatures were retained during subduction and reflect anoxic conditions during deep-sea sedimentation in the Mid-Proterozoic. Finally, Mo isotope fractionation between different terrestrial reservoirs likely depends on the slab redox budget, and therefore on the timing of subduction with regard to Earth's surface oxygenation.

Introduction

The quantification of element- and isotope fractionation in subduction zones plays an important role in understanding (re)cycling mechanisms between the Earth's surface and its interior over geologic time-scales. Element and isotope fractionation in this setting can be controlled by the prevailing redox conditions of the subducted material. As aerobic conditions prevail at the Earth's surface today, deep-sea sediments and altered oceanic crust (AOC) are largely oxidised and influence the redox budget of the subducting slab (*e.g.* Evans, 2012). It is still unclear whether the redox budget of slabs is directly correlated with the oxygenation of Earth's atmosphere and oceans, and whether the redox state of the Earth's surface influences the behaviour of redox-sensitive elements in subduction zone settings through Earth's history.

A particularly suitable element to study the relationship between oxidized and reduced geochemical reservoirs is the redox-sensitive element Mo. The mobility of Mo from the subducted material is controlled by the redox-state of slab-derived aqueous fluids and hydrous melts (Bali et al., 2012; Skora et al., 2017). Significant Mo mobilisation and isotope fractionation has been observed during subduction of oxidised lithologies, leaving behind a

Mo-depleted and isotopically light residual slab (*e.g.* Ahmad *et al.*, 2021; Chen *et al.*, 2019; Freymuth *et al.*, 2015; König *et al.*, 2016). Under reducing conditions, only limited Mo mobility is expected to occur in subducted lithologies (Bali et al., 2012; Skora et al., 2017) thus preserving pre-subducted Mo signatures of the surface. This redox-dependent mobilisation of Mo during subduction metamorphism potentially allows reconstructing the redox budget of ancient subduction zones through Mo isotope compositions of mantle derived material enriched by ancient recycled crustal components.

This study investigates Mo isotope systematics in a well-characterised basaltic sample suite from the South Mid-Atlantic ridge (S-MAR) that shows evidence for interaction with the enriched Shona and Discovery mantle plumes (Section S-1, Fig. S-1). Previous studies on these samples suggested recycling of ancient oceanic crust and sediments in their mantle source with an age between 1 and 2 Ga based on radiogenic isotopes, and the absence of mass-independent fractionation of S isotopes (Andres et al., 2002; Douglass et al., 1999; Labidi et al., 2013). These basalts additionally feature increasingly heavier S and Se isotope compositions with indicators of mantle source enrichment, and are interpreted to reflect subduction recycling of reduced sediments from a redox-stratified Proterozoic ocean (Labidi et al., 2013; Yierpan *et al.*, 2020).

Results

The $\delta^{98/95}$Mo signatures of S-MAR basaltic glass samples range between -0.24 ‰ and -0.10 ‰. These $\delta^{98/95}$Mo values show correlations with $^{87}Sr/^{86}Sr$ as well as $^{143}Nd/^{144}Nd$, $^{176}Hf/^{177}Hf$ and $\delta^{82/76}$Se (Fig. 1, Fig. S-4a, b). The correlations indicate that Mo isotopes trace mantle source enrichment. The range in $\delta^{98/95}$Mo of the samples is similar to that of MORBs (and seamounts) from the East Pacific Rise (EPR), the Pacific-Antarctic ridge (PAR), and the Mohns Knipovich ridge (MKR; Fig. 1, Fig. S-2). However, the samples from the S-MAR show a much larger variability in $^{87}Sr/^{86}Sr$ and $^{143}Nd/^{144}Nd$ and more systematic source enrichments (Fig. 1, Fig. S-2, Fig. S-4a, b).

Table 1: Average Mo isotope composition of MORBs from the S-MAR and PAR together with radiogenic isotope data (Douglass et al., 1999) *and Se isotope compositions* (Yierpan et al., 2020). *Individual measurements are listed in Table S-1.*

Sample	Type	$\delta^{98/95}$Mo (‰)[A]	n	$\delta^{82/76}$Se (‰)[B]	$^{87}Sr/^{86}Sr$	$^{143}Nd/^{144}Nd$
	Southern Mid-Atlantic ridge					
EW9309 40D-1g	Depleted N-MORB	-0.231	3	-0.18	0.702997	0.513033
EW9309 33D-1g	Discovery influenced MORB (North)	-0.098	3	-0.03	0.704475	0.512726
EW9309 28D-1g	Discovery influenced MORB (North)	-0.239	2	-0.14	0.703028	0.513077
EW9309 2D-1g	Discovery influenced MORB (South)	-0.148	2	-0.08	0.704127	0.512652
EW9309 4D-3g	Discovery influenced MORB (South)	-0.152	3	-0.04	0.703762	0.512732
EW9309 9D-3g	LOMU MORB	-0.183	2	-0.03	0.704284	0.512873
EW9309 15D-1g	Shona influenced MORB	-0.207	2	-0.13	0.702741	0.513008
EW9309 21D-1g	Shona influenced MORB	-0.188	2	-0.12	0.703115	0.512818
EW9309 22D-3g	Shona influenced MORB	-0.187	2	-0.08	0.703576	0.512893
	Pacific-Antarctic ridge					
PAC2 DR33-1	Depleted N-MORB	-0.245	3	-0.15	0.702488	0.513082
PAC1 CV-02g	Depleted N-MORB	-0.297	3	-0.23	0.702568	0.513135

[A] The external reproducibility (2 SD) is 0.05 ‰ (supplementary section S-4).

[B] The external reproducibility (2 SD) is 0.08 ‰, except for EW9309 2D-1g and EW9309 9D-3g where it is 0.04 ‰ (Yierpan et al., 2020).

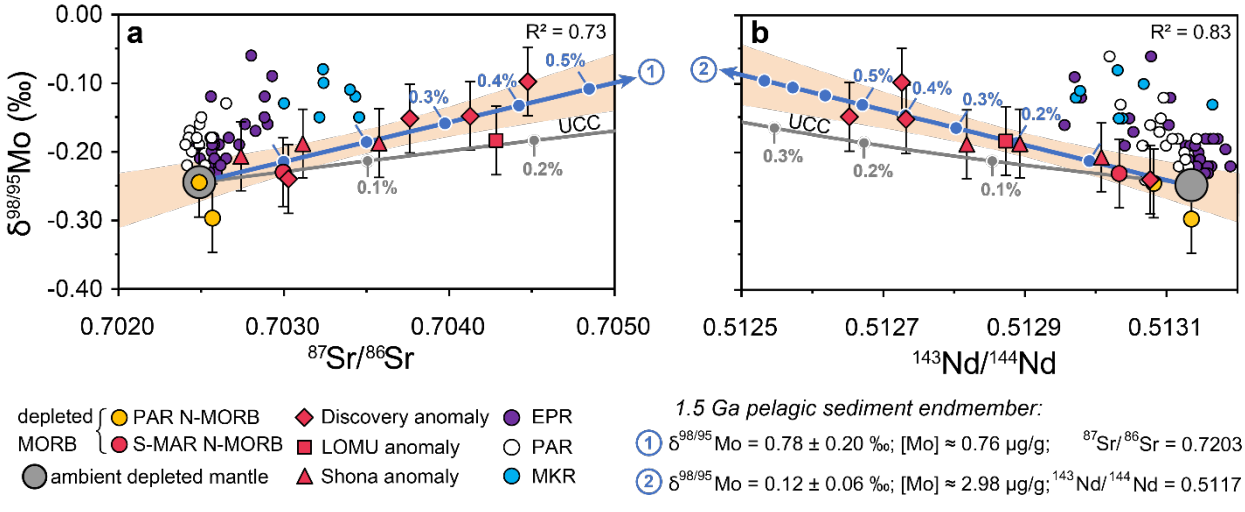

Figure 1: Covariation diagram of MORBs: (a) $\delta^{98/95}$Mo vs. ^{87}Sr/^{86}Sr; (b) $\delta^{98/95}$Mo vs. ^{143}Nd/^{144}Nd. Mixing of a 1.5 Ga old pelagic sediment endmember (best-fit parameters from linear regression) with the ambient depleted mantle (See Table S-2 for mixing parameters). Mixing with upper continental crust (UCC) is plotted for comparison. External reproducibility on each isotope value is considered for regression, and shaded area indicates 95% CI error envelope. PAR samples are excluded from regression. Error bars indicate 2SD standard deviation external reproducibility.

Discussion

Origin of enriched mantle component

Combined element- and isotope systematics of S-MAR samples strongly suggest that secondary mantle melting processes (such as sulphide melt segregation and fractional crystallization), or seawater alteration, are unlikely the causes for the observed Mo isotope variations. This is because all these processes would have obliterated any correlation between Mo isotope composition and radiogenic isotopes (see supplementary section S-2 for further discussion). Low degree melting of mantle plume material has been suggested to affect geochemical signatures of investigated samples (le Roux et al., 2002), and might have affected their $\delta^{98/95}$Mo (*e.g.* Chen et al., 2022). We argue that this process did not result in a first order modification of the enriched source signatures of our samples. Their distinct radiogenic isotope compositions, their covariation with stable Se and S signatures, and trace element systematics are independent of partial melting variations, suggesting the plume source was enriched prior low-degree mantle melting (le Roux et al., 2002; Labidi et al., 2013; Yierpan et al., 2020). Moreover, the absence of a covariation of $\delta^{98/95}$Mo and Pb isotopes (Fig S-4c, d) does not support the influence of an ancient low degree melt (Chen et al., 2022). Rather, a recycled sediment component can explain the Pb isotope signature of LOMU-affinity samples (cf. Douglass et al., 1999; Andres et al., 2002). In addition, mantle melting degrees of 2.5 % (le Roux et al., 2002) cannot explain the observed variations of $\delta^{98/95}$Mo indicating that heavy Mo is likely a characteristic primary signature of the enriched plume material (see supplementary section S-2 for further details). Previous studies attributed this correlation to the influence of a recycled component, such as delaminated subcontinental lithospheric mantle, lower continental crust, or subducted sediment (±AOC) (Andres et al., 2002; Douglass et al., 1999; le Roux et al., 2002). In line with previous investigations showing covariations between other redox-sensitive stable Se-S isotope systematics and radiogenic isotopes (Labidi *et al.*, 2013; Yierpan

et al., 2020), we suggest that a sediment contribution to the S-MAR mantle source is the most likely scenario for the observed heavy Mo isotope enrichment in our samples (see supplementary section S-3 for further discussion). This sedimentary source was previously inferred to have a mid-Proterozoic age (1 to 2 Ga; Andres *et al.*, 2002; Douglass *et al.*, 1999; Labidi *et al.*, 2013; Yierpan *et al.*, 2020).

Mobility of Mo during subduction: The role of fO_2

Recycled Proterozoic sediments that enriched the S-MAR mantle source with isotopically heavy Mo are in stark contrast to inferred, isotopically light Mo in dehydration residues of subducting Phanerozoic metasediments (Ahmad et al., 2021). The trend towards higher observed (co-) variations of $\delta^{98/95}$Mo with increasing degrees of mantle source enrichment within the S-MAR suite therefore implies recycling of a sedimentary $\delta^{98/95}$Mo or even total Mo budget unaffected by dehydration and melting during subduction. This may be reconciled with experimental studies showing immobility of Mo in low fO_2-bearing slab fluids and hydrous slab melts (Bali et al., 2012; Chowdhury et al., 2022; Skora et al., 2017). These experiments were conducted at subduction zone P-T and at reducing conditions, and showed that Mo^{4+} is immobile in fluids in the presence of rutile (Bali et al., 2012) and mobilization of Mo is inefficient in melts due to increased partitioning of Mo^{4+} relative to Mo^{6+} into the residual phases such as sulphides or rutile (Chowdhury et al., 2022; Skora et al., 2017). These findings are also consistent with subduction of OM-rich black shales in the Lesser Antilles arc, where lavas south of Martinique exhibit high $\delta^{98/95}$Mo along with lower Mo/Ce (Freymuth et al., 2016; Gaschnig et al., 2017), suggesting the minute contribution of unfractionated slab-derived Mo to the mantle sources relative to melts originating from more oxidising sediments. Therefore, significant loss of heavy Mo during subduction metamorphism did not occur in the enriched mantle source component. This would have resulted in a preferential loss of more incompatible (isotopically heavy) Mo^{6+} during melting and dehydration (*e.g.* McCoy-West et al., 2019; Chen et al., 2019) and would shift $\delta^{98/95}$Mo of the residual subducted material towards lighter values. The interpretation is in line with the fO_2-sensitive stable isotope systematics of S and Se (Table 1), which indicate negligible mobilisation and isotope fractionation during subduction (Labidi et al., 2013; Yierpan et al., 2020). It is noteworthy that in some cases, that do not apply here, sediments may also buffer subduction zone fluids towards oxidising conditions, such as Fe- and Mn-rich (meta)sediments that show a high metamorphic fO_2 (Ague *et al.*, 2022 and references therein). Yet, our S-MAR data can be attributed to an immobile behaviour of Mo with unchanged $\delta^{98/95}$Mo under reducing conditions, which is in sharp contrast with the

mobility of Mo under oxidising conditions where prograde subduction metamorphism can cause Mo mobilisation and alter the primary slab Mo isotope signature.

Recycled sediments from an anoxic deep-ocean

The $\delta^{98/95}$Mo-^{87}Sr/^{86}Sr-^{143}Nd/^{144}Nd covariations (Fig. 1) in the S-MAR data combined with the previously established model of linear δ^{34}S-δ^{82}Se-^{87}Sr/^{86}Sr(-^{143}Nd/^{144}Nd) relationship (Labidi et al., 2013; Yierpan et al., 2020) allows extrapolation of $\delta^{98/95}$Mo and [Mo] to constrain the nature of the recycled sediment. Extrapolation of the linear regression to a model composition of 1.5-Ga-old sediment (^{87}Sr/^{86}Sr = 0.7203, ^{143}Nd/^{144}Nd = 0.5117; Fig. 1, see Table S-2 for details) yields two vastly different endmember Mo signatures with $\delta^{98/95}$Mo of 0.78 ± 0.20 ‰ and 0.12 ± 0.06 ‰, and [Mo] of ~ 0.76 µg/g and 2.98 µg/g, respectively (see blue mixing lines in Fig. 1a+b). This indicates that the linear extrapolation might not sufficiently constrain the Mo composition of the recycled sediment source. Considering the present-day ^{87}Sr/^{86}Sr and ^{143}Nd/^{144}Nd model composition of 1.5-Ga-old subducted sediment, the isotopic variations of the samples represents only a small fraction of the mixing space between the ambient depleted mantle and recycled sediment. Therefore, for given radiogenic Nd and Sr signatures of the sedimentary component, different $\delta^{98/95}$Mo and [Mo] combinations can potentially result in a minimum least squares error between the mixing model and the S-MAR data. As both variables cannot be independently constrained, a misfit function (supplementary section S-5) was applied to calculate the sedimentary $\delta^{98/95}$Mo and [Mo] that represent the measured $\delta^{98/95}$Mo-^{87}Sr/^{86}Sr-^{143}Nd/^{144}Nd covariation best (Fig. 2).

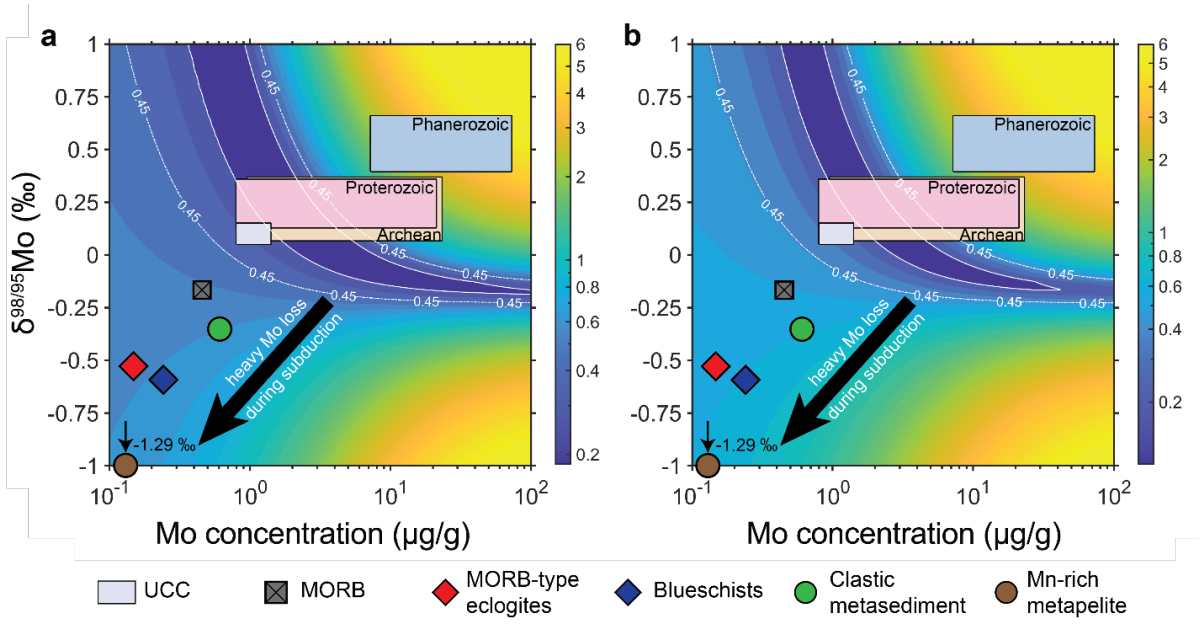

Figure 2: Least squares error ($\Delta^{98/95}$Mo in ‰; up to 6 ‰) between calculated mixing lines and analysed samples. Variables are (a) the $\delta^{98/95}$Mo and [Mo]) values derived from the $\delta^{98/95}$Mo vs. $^{87}Sr/^{86}Sr$ and (b) $\delta^{98/95}$Mo vs. $^{143}Nd/^{144}Nd$ relationship (Fig. 1). Literature values for potential (concentration averaged) recycled lithologies, and anoxic sediments sorted by age intervals are shown for comparison. See Table S-2 and supplementary section S-5 for references, mixing parameters, and further details.

Least squares errors for variable $\delta^{98/95}$Mo and [Mo] values for a given 1.5 Ga old sediment with $^{143}Nd/^{144}Nd$ and $^{87}Sr/^{86}Sr$ endmember values (blue field in Fig. 2) show a similar pattern for both radiogenic isotope systems, which indicates that a Mid-Proterozoic pelagic sediment is likely to be a valid endmember. Best fits with minimum errors overlap with the lower 1*s* of Proterozoic OM-rich sediment data from the literature (Ye *et al.*, 2021; Table S-2) and can also be achieved with a recycled sediment contribution close to that of the UCC (~ 0.15 ‰; Willbold and Elliott, 2017 and references therein) with slightly higher $\delta^{98/95}$Mo and/or [Mo] values. This points towards a minor authigenic Mo enrichment from seawater or a residual enrichment of Mo (*e.g.* Kendall et al., 2017) and implies that $\delta^{98/95}$Mo has not been affected by oxic conditions during slab dehydration due to subduction of reducing lithologies (Fig. 2).

These findings support the notion that the deep-ocean remained anoxic until the beginning of the Phanerozoic (*e.g.* Poulton and Canfield, 2011; Stolper and Keller, 2018). The extent of the biological pump in the Proterozoic ocean, where primary productivity in oxygenated surface ocean was dominated by cyanobacteria, was lower compared to modern oceans and higher primary surface productivity was restricted to marine environment close to continents (Laakso and Schrag, 2019). This limited the OM-flux to the Proterozoic deep-ocean and therefore authigenic Mo accumulation from seawater. However, deep-ocean anoxic conditions increased OM-preservation and burial efficiency (Burdige, 2007). Furthermore, under anoxic conditions with an overall low concentration of dissolved SO_4^{2-} and MoO_4^{2-}, neither a significant Mo enrichment from seawater into the sediment nor a significant Mo mobilisation during fluid alteration is expected (Lyons et al., 2014). The overall lower OM-input to the deep-ocean and smaller oceanic Mo reservoir can therefore explain the small authigenic heavy Mo contribution to the recycled Mid-Proterozoic deep-sea sediment (Fig. 2). With respect to the much shorter ocean residence time of Mo relative to the average lifetime of an oceanic crust, the S-MAR enriched endmember is likely representative for overall reducing conditions during subduction

an average subducted sedimentary Mo signature, which provides a context of deep-ocean redox conditions.

Implications for the sedimentary Mo subduction cycle

Due to the anoxic conditions in the Proterozoic deep ocean, oxidised species of major and minor elements like Fe, S and Mn, were absent in deep-sea sediments, thus lowering their redox budget/oxidising capacity compared to present-day marine lithologies (*e.g.* Ague *et al.*, 2022; Evans, 2012). This may also explain the preserved $\delta^{98/95}$Mo of a reduced Proterozoic sediment component recycled into the S-MAR mantle source, in contrast to Neo-Proterozoic, deep mantle recycling of low $\delta^{98/95}$Mo into mantle plume sources (see also Ma *et al.*, 2022). This is in line with Samoan OIBs, where $\delta^{98/95}$Mo signatures are interpreted as a mixture of isotopically heavy terrigenous sediments ($\delta^{98/95}$Mo ≈ UCC) and isotopically light dehydrated mafic oceanic crust, which reflect the influence of a distinct pool of Mid-Proterozoic recycled ocean crust (Gaschnig et al., 2021). Altogether, this indicates that changing Earth surface redox conditions have influenced the fO_2 conditions during subduction and the mobility of sedimentary Mo (and by analogy that of other redox-sensitive elements) and hence, the Mo isotope budget between different Earth (silicate) reservoirs. This emphasises the time- and condition-related variations in Mo mobility during subduction on our planet (Fig. 3). We therefore conclude that the Mo isotope signature of plume-influenced volcanic rocks can be used to reconcile the redox conditions during ancient surface deposition of deep-sea sediments (cf. Gaschnig *et al.*, 2021) as well as during subduction-related prograde metamorphism and the inception of modern subduction.

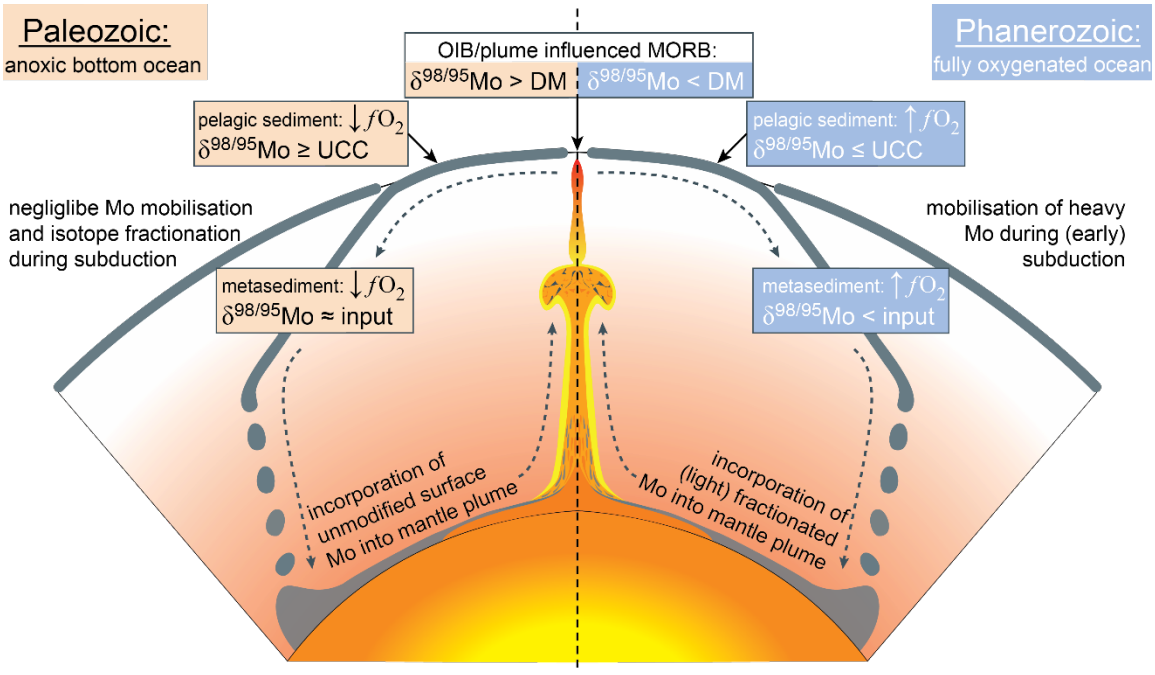

Figure 3: Illustration of the subducted sedimentary Mo cycle during the Paleozoic (left) and Phanerozoic (right). Deep-sea sediment carry variable redox budgets influencing Mo mobility and hence isotope fractionation during subduction over Earth's history (see text). UCC = upper continental crust. DM = Depleted Mantle.

Acknowledgements

This work was funded by the Swiss National Science Foundation, Switzerland (Grant number 182508) to M.W. The MC-ICP-MS at the Institute of Geological Sciences, University of Bern used in this study was acquired within the framework of the NCCR project PlanetS (Grant nr. 1NF40-141881) funded by the Swiss National Science Foundation. S.K. and C.R. acknowledge ERC Starting Grant 636808 (project O_2RIGIN). S.K also acknowledges Ramón y Cajal contract RYC2020-030014-I. Jörg Hermann and Paolo Sossi are acknowledged for discussions that contributed to this manuscript. We also wish to thank Alex McCoy-West and 2 anonymous reviewers for constructive reviews, as well as Helen Williams for editorial handling.

References

Ague, J.J., Tassara, S., Holycross, M.E., Li, J.-L., Cottrell, E., Schwarzenbach, E.M., Fassoulas, C., John, T., 2022. Slab-derived devolatilization fluids oxidized by subducted metasedimentary rocks. Nat. Geosci. 2022 1–7. https://doi.org/10.1038/s41561-022-00904-7

Ahmad, Q., Wille, M., König, S., Rosca, C., Hensel, A., Pettke, T., Hermann, J., 2021. The Molybdenum isotope subduction recycling conundrum: A case study from the Tongan subduction zone, Western Alps and Alpine Corsica. Chem. Geol. 576, 120231. https://doi.org/10.1016/J.CHEMGEO.2021.120231

Andres, M., Blichert-Toft, J., Schilling, J.-G., 2002. Hafnium isotopes in basalts from the southern Mid-Atlantic Ridge from 40°S to 55°S: Discovery and Shona plume–ridge interactions and the role of recycled sediments. Geochemistry, Geophys. Geosystems 3, 1–25. https://doi.org/10.1029/2002GC000324

Bali, E., Keppler, H., Audetat, A., 2012. The mobility of W and Mo in subduction zone fluids and the Mo-W-Th-U systematics of island arc magmas. Earth Planet. Sci. Lett. 351–352, 195–207. https://doi.org/10.1016/j.epsl.2012.07.032

Burdige, D.J., 2007. Preservation of organic matter in marine sediments: controls, mechanisms, and an imbalance in sediment organic carbon budgets? Chem. Rev. 107, 467–485.

https://doi.org/10.1021/CR050347Q

Chen, S., Hin, R.C., John, T., Brooker, R., Bryan, B., Niu, Y., Elliott, T., 2019. Molybdenum systematics of subducted crust record reactive fluid flow from underlying slab serpentine dehydration. Nat. Commun. 10. https://doi.org/10.1038/s41467-019-12696-3

Chen, S., Sun, P., Niu, Y., Guo, P., Elliott, T., Hin, R.C., 2022. Molybdenum isotope systematics of lavas from the East Pacific Rise: Constraints on the source of enriched mid-ocean ridge basalt. Earth Planet. Sci. Lett. 117283. https://doi.org/10.1016/J.EPSL.2021.117283

Chowdhury, P., Dasgupta, R., Phelps, P.R., Costin, G., Lee, C.-T.A., 2022. Oxygen fugacity range of subducting crust inferred from fractionation of trace elements during fluid-present slab melting in the presence of anhydrite versus sulfide. Geochim. Cosmochim. Acta. https://doi.org/10.1016/J.GCA.2022.02.030

Douglass, J., Schilling, J.-G., Fontignie, D., 1999. Plume-ridge interactions of the Discovery and Shona mantle plumes with the southern Mid-Atlantic Ridge (40°-55°S). J. Geophys. Res. Solid Earth 104, 2941–2962. https://doi.org/10.1029/98JB02642

Evans, K.A., 2012. The redox budget of subduction zones. Earth-Science Rev. 113, 11–32. https://doi.org/10.1016/J.EARSCIREV.2012.03.003

Freymuth, H., Elliott, T., van Soest, M., Skora, S., 2016. Tracing subducted black shales in the Lesser Antilles arc using molybdenum isotope ratios. Geology 44, 987–990. https://doi.org/10.1130/G38344.1

Freymuth, H., Vils, F., Willbold, M., Taylor, R.N., Elliott, T., 2015. Molybdenum mobility and isotopic fractionation during subduction at the Mariana arc. Earth Planet. Sci. Lett. 432, 176–186. https://doi.org/10.1016/j.epsl.2015.10.006

Gaschnig, R.M., Reinhard, C.T., Planavsky, N.J., Wang, X., Asael, D., Chauvel, C., 2017. The Molybdenum Isotope System as a Tracer of Slab Input in Subduction Zones: An Example From Martinique, Lesser Antilles Arc. Geochemistry, Geophys. Geosystems 18, 4674–4689. https://doi.org/10.1002/2017GC007085

Gaschnig, R.M., Reinhard, C.T., Planavsky, N.J., Wang, X., Asael, D., Jackson, M.G., 2021. The impact of primary processes and secondary alteration on the stable isotope composition of ocean island basalts. Chem. Geol. 581, 120416. https://doi.org/10.1016/J.CHEMGEO.2021.120416

Kendall, B., Dahl, T.W., Anbar, A.D., 2017. Good Golly, Why Moly? The stable isotope geochemistry of molybdenum, in: Non-Traditional Stable Isotopes. Walter de Gruyter GmbH, pp. 683–732. https://doi.org/10.2138/rmg.2017.82.16

303 König, S., Wille, M., Voegelin, A., Schoenberg, R., 2016. Molybdenum isotope systematics in
304 subduction zones. Earth Planet. Sci. Lett. 447, 95–102.
305 https://doi.org/10.1016/j.epsl.2016.04.033
306 Laakso, T.A., Schrag, D.P., 2019. A small marine biosphere in the Proterozoic. Geobiology
307 17, 161–171. https://doi.org/10.1111/GBI.12323
308 Labidi, J., Cartigny, P., Moreira, M., 2013. Non-chondritic sulphur isotope composition of the
309 terrestrial mantle. Nat. 2013 5017466 501, 208–211. https://doi.org/10.1038/nature12490
310 le Roux, P.J., Le Roex, A.P., Schilling, J.G., Shimizu, N., Perkins, W.W., Pearce, N.J.G., 2002.
311 Mantle heterogeneity beneath the southern Mid-Atlantic Ridge: trace element evidence
312 for contamination of ambient asthenospheric mantle. Earth Planet. Sci. Lett. 203, 479–
313 498. https://doi.org/10.1016/S0012-821X(02)00832-4
314 Lyons, T.W., Reinhard, C.T., Planavsky, N.J., 2014. The rise of oxygen in Earth's early ocean
315 and atmosphere. Nat. 2014 5067488 506, 307–315. https://doi.org/10.1038/nature13068
316 Ma, L., Xu, Y.G., Li, J., Chen, L.H., Liu, J.Q., Li, H.Y., Huang, X.L., Ma, Q., Hong, L.B.,
317 Wang, Y., 2022. Molybdenum isotopic constraints on the origin of EM1-type continental
318 intraplate basalts. Geochim. Cosmochim. Acta 317, 255–268.
319 https://doi.org/10.1016/J.GCA.2021.11.013
320 Skora, S., Freymuth, H., Blundy, J., Elliott, T., Guillong, M., 2017. An experimental study of
321 the behaviour of cerium/molybdenum ratios during subduction: Implications for tracing
322 the slab component in the Lesser Antilles and Mariana Arc. Geochim. Cosmochim. Acta
323 212, 133–155. https://doi.org/10.1016/j.gca.2017.05.025
324 Stolper, D.A., Keller, C.B., 2018. A record of deep-ocean dissolved O_2 from the oxidation state
325 of iron in submarine basalts. Nat. 2018 5537688 553, 323–327.
326 https://doi.org/10.1038/nature25009
327 Willbold, M., Elliott, T., 2017. Molybdenum isotope variations in magmatic rocks. Chem.
328 Geol. 449, 253–268. https://doi.org/10.1016/j.chemgeo.2016.12.011
329 Ye, Y., Zhang, S., Wang, H., Wang, X., Tan, C., Li, M., Wu, C., Canfield, D.E., 2021. Black
330 shale Mo isotope record reveals dynamic ocean redox during the Mesoproterozoic Era.
331 Geochemical Perspect. Lett. 18, 16–21. https://doi.org/10.7185/GEOCHEMLET.2118
332 Yierpan, A., König, S., Labidi, J., Schoenberg, R., 2020. Recycled selenium in hot spot–
333 influenced lavas records ocean-atmosphere oxygenation. Sci. Adv. 6, eabb6179.
334 https://doi.org/10.1126/SCIADV.ABB6179
335

Geochemical Perspectives Letters

Molybdenum isotopes in plume-influenced MORBs reveal recycling of ancient anoxic sediments

Q. Ahmad, M. Wille, C. Rosca, J. Labidi, T. Schmid, K. Mezger, S. König

Supplementary Information

The Supplementary Information includes:

Section S-1: Geochemical background of the samples

The studied samples are fresh basaltic glasses that were dredged from the South-Mid Atlantic Ridge (S-MAR) during the R/V Maurice Ewing cruise EW93-09 (Douglass et al., 1999, 1995). All samples were well-characterized in terms of radiogenic isotopes (Sr, Nd, Hf, and Pb) (Andres et al., 2002; Douglass et al., 1999), S isotopes (Labidi et al., 2013), Se isotopes (Yierpan et al., 2020), noble gases (Moreira et al., 1995; Sarda et

al., 2000) and major and trace element abundances (Kelley et al., 2013; le Roux et al., 2002c, 2002b, 2002a). This makes the selected sample suite ideal for investigating their Mo isotope signature.

The most prominent feature in the S-MAR is the localised interaction between the ambient asthenospheric mantle and the Discovery and Shona mantle plumes (Fig. S-1). A variety of recycled components have been suggested to be incorporated in these mantle plumes based on radiogenic and stable isotope systematics (Fig. S-2; see references above).

Two additional samples from the Pacific-Antarctic Ridge (PAR) complement existing PAR-MORB Mo isotope data (Bezard et al., 2016). This setting is dominantly sourced by depleted mantle being devoid of any deep mantle plume influence (*e.g.* Hamelin *et al.*, 2011) with radiogenic Sr and Nd isotope signature similar to the ambient depleted mantle (ADM) constrained for the S-MAR suite (Table S-1; Andres et al., 2002; Douglass et al., 1999).

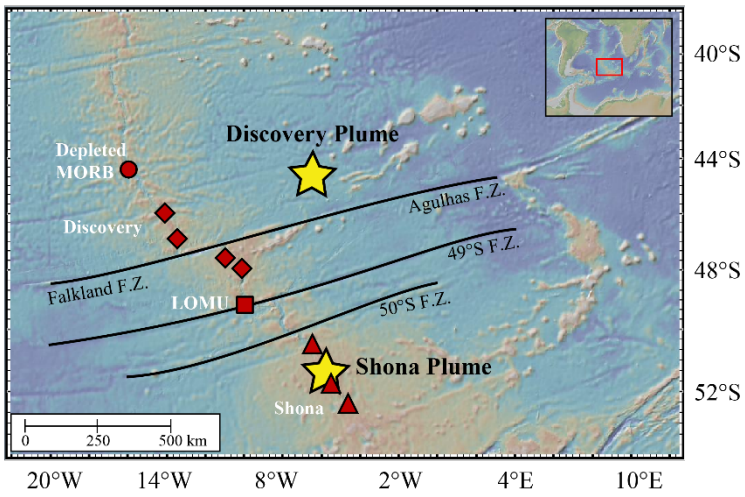

Figure S-1: Sample locations along the S-MAR together with the Discovery and Shona plume, as well as tectonic fracture zones (F.Z.). Figure made with GeoMapApp (www.geomapapp.org).

Section S-2: Potential controls on the Mo isotope variability of S-MAR basalts

Observed correlations between $\delta^{98/95}$Mo and ^{143}Nd/^{144}Nd or ^{176}Hf/^{177}Hf (Fig. 1, S-4a) exclude post-emplacement seawater alteration effects on the Mo isotope composition, as seawater incorporation is insensitive to relatively fluid-immobile Nd or Hf (cf. Labidi et al., 2013). This is also supported by Cl/K ratios close to the range of global MORB (Table S-1) (Labidi et al., 2013). Also unlikely is isotope fractionation due to segregation of an isotopically heavy sulphide melt at low melting degrees, which results into an isotopically light silicate melt (Liang et al., 2017). The studied samples were sulphide-saturated during melting (Labidi *et al.*, 2013 and references therein), however, there is no correlation between $\delta^{98/95}$Mo and Mo/Ce with Ce being

similarly incompatible during mantle melting, but Mo being more compatible in presence of a segregated sulphide melt. Furthermore, a potential sulphide melt segregation would have removed any relationship between $\delta^{98/95}$Mo, and radiogenic isotopes (cf. Labidi *et al.*, 2013). This covariation together with lack of covariations between $\delta^{98/95}$Mo and MgO or Mg#, overall high MgO contents (Table S-1) suggests that also fractional crystallisation during differentiation is not the cause of the observed Mo isotope variation (*e.g.* Voegelin et al., 2014). This is in line with other tholeiitic systems (*e.g.* Bezard et al., 2016; Yang et al., 2015).

Elemental systematics of S-MAR basalts suggest mixing of ambient mantle with low-degree melts (F = 2-3 %; le Roux *et al.*, 2002a). Previously, elevated $\delta^{98/95}$Mo in lavas from the EPR (devoid of a mantle plume component) were interpreted to reflect mixing of depleted MORB with an isotopically heavy endmember of magmatic origin without contribution of recycled components (Chen et al., 2022). The authors argued that this heavy endmember is an ancient (> 1 Ga) low-degree melt (F = 0.2 %) of depleted mantle material that led to an initial fractionation of $\delta^{98/95}$Mo (due to different magmatic compatibilities of Mo^{4+} and Mo^{6+}; McCoy-West et al., 2019), similar incompatible elements (*e.g.* Nb/Zr) and further parent-daughter ratios of radiogenic isotopes. This explains the observed correlation of $\delta^{98/95}$Mo and radiogenic isotopes of Pb, Nd, and Sr (Chen et al., 2022). In the S-MAR sample suite, the trace element ratios are accompanied by radiogenic isotope systematics attributable to an enriched mantle 1 (EM1) signature requiring a higher initial Rb/Sr, lower Sm/Nd and Lu/Hf, and similar U/Pb compared to DMM (Fig. S-2). These signatures, however, are primary and cannot be explained by low-F melting of plume mantle material (le Roux et al., 2002). Furthermore, plume-material is pre-enriched in isotopically heavy S and Se prior to low-F melting (Labidi et al., 2013; Yierpan et al., 2020). The question remains, if heavy Mo is primary or if it is generated during low-F mantle melting. If we consider a low-F melting of F=2.5 % melting (le Roux et al., 2002) of plume material (T = 1200 °C; $Mo^{6+}/\Sigma Mo = 0.99$), we would expect a maximum isotope shift of $\Delta^{98/95}Mo_{max}$ of ~ 0.085 ‰ between pyroxenite melt and DMM (F=15 %). A mixture of both of these endmembers with 20% pyroxenite contribution in our heaviest sample EW9309 33D-1g (le Roux et al., 2002) would lead to a maximum $\Delta^{98/95}Mo_{max}$ of 0.059 ‰ (melting model from Wang & Becker (2018)). This value is likely lower ($\Delta^{98/95}Mo_{max} = 0.040$ ‰) when considering lower N-MORB like [Mo] of pyroxenite melts, as there is no covariation of $\delta^{98/95}$Mo and Mo/Ce. Moreover, these pyroxenites are formed along the plume-adiabat, which is hotter than the N-MORB adiabat, lowering further the isotopic fractionation induced by low-F melting. Furthermore, we do not observe a correlation of $\delta^{98/95}$Mo with Pb isotopes, which is inconsistent with the increase of U/Pb during ancient low-F melting (Chen et al., 2022). In contrast, we observe LOMU-samples that carry an isotopic heavy signature, which is consistent with an *e.g.* Proterozoic sediment contribution (*e.g.* Rehkämper & Hofmann, 1997; Douglass et al., 1999; Andres et al., 2003). As correlations between radiogenic isotopes and $\delta^{34/32}$S, $\delta^{82/76}$Se, and $\delta^{98/95}$Mo (*e.g.* Fig. 1, S-4b)

cannot be explained by magmatic processes or post-emplacement alteration (c.f. Labidi *et al.*, 2013; Yierpan *et al.*, 2020), this relationship is in strong support of recycling of enriched mantle components with $\delta^{98/95}$Mo> depleted mantle.

Section S-3: Origin of enriched mantle

Different recycled components (*e.g.* sub-continental mantle, lower continental crust, oceanic crust, and sediment) in the mantle source of the S-MAR (Andres et al., 2002; Douglass et al., 1999; Labidi et al., 2013; le Roux et al., 2002c; Yierpan et al., 2020) can have an influence on $\delta^{98/95}$Mo of the samples. Sub-continental mantle can be excluded as a significant component, since worldwide peridotites have a MORB-like $\delta^{98/95}$Mo (-0.206 ± 0.05‰; Liang *et al.*, 2017). An aqueous fluid expelled from subducted crust can influence the mantle composition leading to elevated $\delta^{98/95}$Mo and [Mo] (*e.g.* Ahmad *et al.*, 2021); however, we observe correlations between $\delta^{98/95}$Mo and aqueous fluid-immobile Nd and Hf isotopes (Fig. 1, Fig. S-4a) and no covariation is observed with fluid proxies, such as Ba/Th ($R^2 = 0.1$). There is no direct estimate of $\delta^{98/95}$Mo of the lower continental crust (LCC), however, cumulates which possibly reside in the LCC, likely incorporate preferentially light Mo isotopes (Nebel-Jacobsen et al., 2021; Wille et al., 2018) and are unsuitable candidates to explain Mo signatures in the basalt samples. Apart from a clear EM1 affinity, two samples analysed here show a trend towards HIMU (Fig. S-2), thus a signature of recycled AOC. However, ^{206}Pb/^{204}Pb ratios do not correlate with $\delta^{98/95}$Mo and most radiogenic ^{206}Pb/^{204}Pb values are accompanied with depleted mantle-like $\delta^{98/95}$Mo (Fig. S-4c). This leads to the conclusion that a significant influence of recycled AOC is unlikely.

Section S-4: Analytical Methods

Molybdenum purification and isotope analysis was conducted in the clean laboratory facilities at the Institute of Geological Sciences, University of Bern. For all samples, enough powder was weighed to have 25 – 50 ng Mo for analysis. The material was spiked with an enriched isotope tracer solution (^{97}Mo-^{100}Mo double spike). The samples were then dissolved in concentrated single-distilled acids in the following sequence: (*i*) concentrated HF-HNO_3 (3:1 mixture), (*ii*) concentrated HNO_3, (*iii*) 6 M HCl in Savillex™ Teflon vials. The dissolved samples were processed through anion- and cation exchange columns to obtain a clean Mo separate (Wille et al., 2013). In the first step, samples were taken up in 4 M HCl and passed through Dowex 1X8, 200-400 mesh, anion resin. In a second step, the sample material was taken up in 0.5 M HCl and passed through Dowex 50WX8 200-400 mesh, cation exchange resin. Stable Mo isotope measurements were carried out on a Neptune Plus MC-ICPMS coupled with an Aridus II desolvating nebulizer with an uptake rate of 100 – 150 $\mu l \cdot min^{-1}$ (details are provided in Ahmad *et al.*, 2021). Six Mo isotopes (^{94}Mo, ^{95}Mo, ^{96}Mo, ^{97}Mo, ^{98}Mo and

^{100}Mo) were measured as well as ^{99}Ru and ^{101}Ru to monitor potential isobaric interference. We used resistors with $10^{-11}\Omega$ to analyse all isotopes except ^{101}Ru, which was measured using a 10^{-12} Ω resistor. For analyses, we have used a combination of 'H' Ni sampler cone and 'X' Ni skimmer cone and obtained ~ 120 V/ppm on ^{95}Mo. We used a double spike correction method based on an iterative calculation procedure (see Siebert *et al.*, 2001). The total procedural blank was between 0.22 to 0.65 ng. We present all data in the δ-notation and relative to NIST SRM 3134 in ‰ (Goldberg et al., 2013; Greber et al., 2012) with an interference correction based on ^{99}Ru:

$$\delta^{98/95}Mo = \left(\frac{\left(\frac{^{98}Mo}{^{95}Mo}\right)_{Sample}}{\left(\frac{^{98}Mo}{^{95}Mo}\right)_{NIST\ SRM\ 3134}} - 1 \right) * 1{,}000 \qquad \text{(S-1)}$$

Interference corrected $\delta^{98/95}$Mo ratios based on ^{99}Ru and ^{101}Ru correction were compared to ensure accurate determination of Ru interference. Background correction was obtained by bracketing samples with measurements of 0.5 M HNO_3 carrier solution on-peak. Sample and background analysis consisted of 80 and 30 cycles, respectively, with a signal integration time of 4.194 s for each cycle. Repeated measurements of the standard NIST SRM 3134 and an in-house J&M standard solution lot 602332B gave an isotopic difference of $\Delta^{98/95}$Mo = 0.269 ± 0.017 ‰ (2 SD, n = 14), in agreement with (Ahmad et al., 2021; Greber et al., 2012). Solution standards were measured at a concentration of 25 ppb. Individually digested and chemically purified whole-rock reference materials AGV-2, BHVO-2 and W-2a yielded a $\delta^{98/95}$Mo of -0.19 ± 0.03 ‰ (2 SD, n = 3), -0.11 ± 0.04 ‰ (2 SD, n = 3) and -0.09 ± 0.05 ‰ (2 SD, n = 3), respectively (Table S-1). The values are within uncertainty of those determined previously (*e.g.* Burkhardt et al., 2014; Willbold et al., 2016; Zhao et al., 2016). Individual measurements of whole rock reference materials (Table S-1) are within the long-term 2SD external reproducibility of ± 0.05 ‰ as determined by previous measurements of BHVO-2 (Ahmad et al., 2021). Including these previous BHVO-2 measurements (-0.09 ± 0.05 ‰; n = 10), we consider ± 0.05 ‰ as the long-term 2SD external reproducibility of our sample measurements. All samples were measured multiple times (after individual digestions and chemical separation) and obtained $\delta^{98/95}$Mo and Mo concentration values were averaged for data presentation and interpretation (Table S-1). All individual sample measurements are within ± 0.05 ‰ compared to their average $\delta^{98/95}$Mo, except PAR sample PAC CV-02g.

Table S-1: Average and individual Mo isotope and elemental data of analysed MORBs from S-MAR and PAR. MgO and calculated Cl/K from (Labidi et al., 2013; le Roux et al., 2002b). Individual measurements represent separate sample digestions and chromatographic separations.*Internal precision on a sample run (over 80 cycles) is reported as 2 standard error (2SE).

		Individual measurement			Mean				
Sample	Type	$\delta^{98/95}$Mo (‰)	2SE* (‰)	Mo (µg/g)	$\delta^{98/95}$Mo (‰)	2SD (‰)	Mo (µg/g)	MgO (wt. %)	Cl/K
	Southern Mid-Atlantic ridge								
EW9309 40D-1g	Depleted N-MORB	-0.226	0.015	0.254	-0.231	0.064	0.254	8.30	0.11
		-0.201	0.022	0.255					
		-0.265	0.020	0.254					
EW9309 33D-1g	Discovery influenced MORB (North)	-0.100	0.013	1.25	-0.098	0.048	1.25	7.83	0.04
		-0.073	0.020	1.25					
		-0.121	0.013	1.25					
EW9309 28D-1g	Discovery influenced MORB (North)	-0.191	0.018	0.168	-0.239	0.136	0.169	8.22	0.06
		-0.287	0.018	0.170					
EW9309 2D-1g	Discovery influenced MORB (South)	-0.122	0.020	0.665	-0.148	0.074	0.663	6.24	0.03
		-0.174	0.014	0.661					
EW9309 4D-3g	Discovery influenced MORB (South)	-0.136	0.015	0.539	-0.152	0.077	0.528	7.60	0.04
		-0.124	0.020	0.527					
		-0.195	0.016	0.517					
EW9309 9D-3g	LOMU MORB	-0.167	0.017	0.654	-0.183	0.045	0.654	8.67	0.06

		-0.199	0.015	0.654					
EW9309 15D-1g	Shona influenced MORB	-0.199	0.028	0.363	-0.207	0.023	0.364	7.81	0.08
		-0.215	0.019	0.364					
EW9309 21D-1g	Shona influenced MORB	-0.179	0.027	0.587	-0.188	0.024	0.586	7.10	0.05
		-0.196	0.013	0.585					
EW9309 22D-3g	Shona influenced MORB	-0.155	0.019	1.03	-0.187	0.090	1.03	4.83	0.07
		-0.219	0.017	1.03					
	Pacific-Antarctic ridge								
PAC2 DR33-1	Depleted N-MORB	-0.225	0.018	0.470	-0.245	0.062	0.462	6.63	-
		-0.228	0.028	0.461					
		-0.281	0.016	0.454					
PAC1 CV-02g	Depleted N-MORB	-0.249	0.016	0.213	-0.297	0.116	0.215	7.74	-
		-0.280	0.031	0.213					
		-0.361	0.021	0.218					
	Rock reference materials								
AGV-2	Andesite	-0.192	0.015	2.13	-0.194	0.042	2.14	-	-
		-0.211	0.019	2.11					
		-0.179	0.012	2.19					
BHVO-2	Basalt	-0.092	0.015	3.43	-0.108	0.032	3.68	-	-
		-0.099	0.017	4.64					
		-0.132	0.015	2.96					
W-2a	Diabase	-0.100	0.018	0.462	-0.087	0.053	0.452	-	-
		-0.104	0.021	0.455					
		-0.057	0.010	0.439					

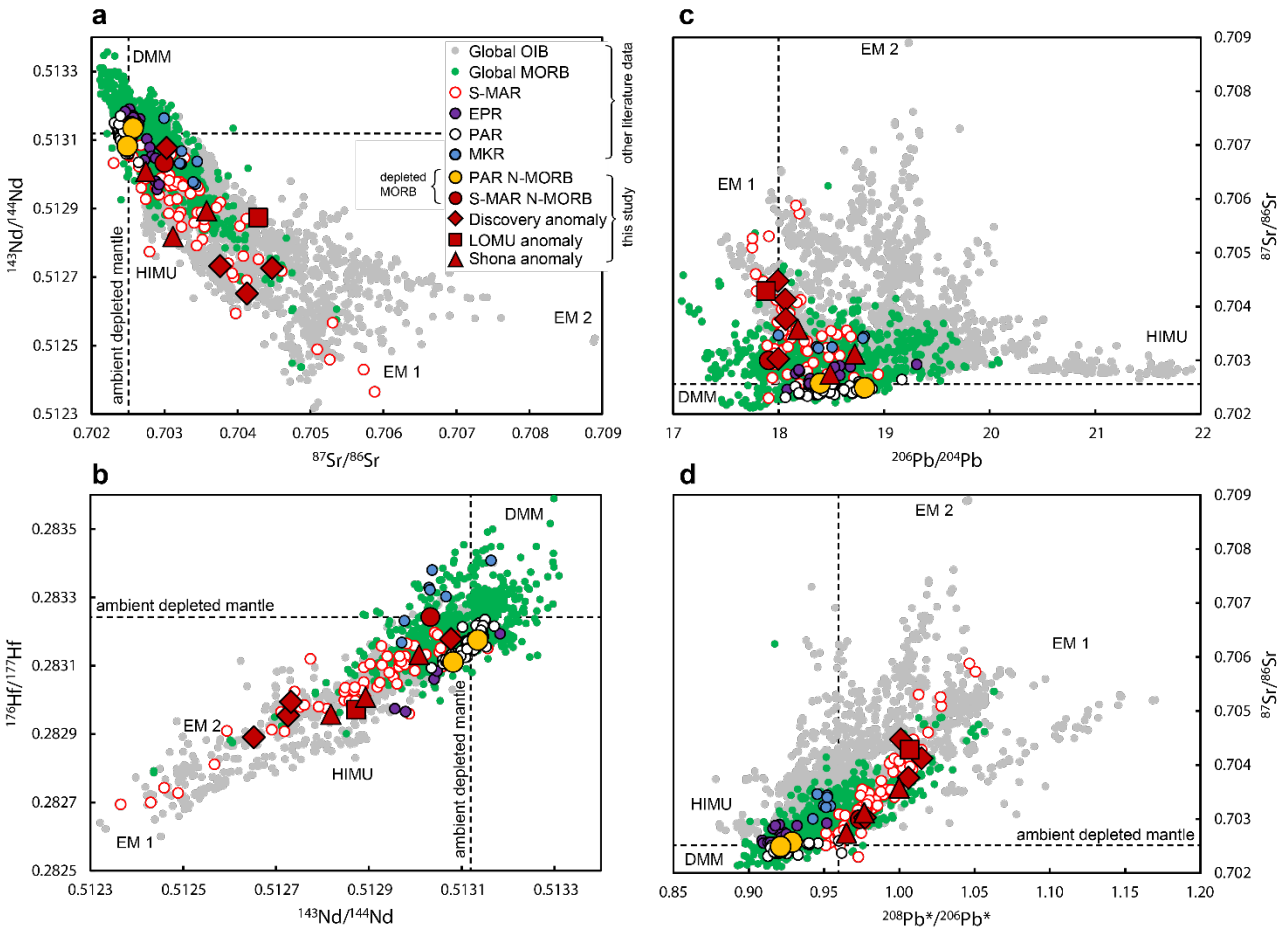

Figure S-2: Radiogenic isotope data for the studied S-MAR and PAR glasses modified after Yierpan *et al.*, (2020). (a-d) Shown for comparison are a global compilation of MORB and OIB (Stracke, 2012 and references therein). MORBs (and seamounts) near the East Pacific Rise (EPR) (Chen *et al.*, 2021 and references therein), Mohns-Knipovich ridges (MKR) (Bezard et al., 2016), and PAR (Hamelin *et al.*, 2011 and references therein) are plotted for comparision. A more detailed precompilation of S-MAR basalts can be found in Labidi *et al.*, (2013). Dashed lines indicate the composition of the S-MAR ambient depleted mantle (Andres et al., 2002; Douglass et al., 1999). (d) $^{208}Pb^*/^{206}Pb^*$ exemplifies the time-integrated Th/U ratios (cf. Stracke, 2012).

Section S-5: Misfit model

The "linear" Mo-Sr(-Nd) isotope sample array (Fig. 1) represents only a small segment relative to the sediment endmember (Table S2), suggesting that a hyperbolic mixing curve could also account for the observed correlation. Mixing of two components (sediment & ambient depleted mantle endmember) with different Mo-Sr(-Nd) isotope compositions and concentrations will result in a hyperbola (cf. Vollmer, 1976) of the form

$$Ax + Bxy + Cy + D = 0 \quad \text{(S-2)}$$

where

$$A = a_{DM}\, b_{SED} y_{DM} - a_{SED} b_{DM} y_{SED} \quad \text{(S-3)}$$
$$B = a_{SED}\, b_{DM} - a_{DM} b_{SED} \quad \text{(S-4)}$$
$$C = a_{DM}\, b_{SED} x_{SED} - a_{SED} b_{DM} x_{DM} \quad \text{(S-5)}$$
$$D = a_{SED}\, b_{DM} x_{DM} y_{SED} - a_{DM} b_{SED} x_{SED} y_{DM} \quad \text{(S-6)}$$

and

$x = {}^{87}Sr/{}^{86}Sr \text{ or } {}^{143}Nd/{}^{144}Nd$
$y = \delta^{98/95}Mo$

$a_{SED} = conc.\,of\ Mo$
$b_{SED} = conc.\,of\ {}^{86}Sr\ (\sim Sr) \text{ or } {}^{144}Nd\ (\sim Nd)$

} of the sediment endmember with the isotopic composition (x_{SED}/y_{SED})

$a_{DM} = conc.\,of\ Mo$
$b_{DM} = conc.\,of\ {}^{86}Sr\ (\sim Sr) \text{ or } {}^{144}Nd\ (\sim Nd)$

} of the depleted mantle endmember with the isotopic composition (x_{DM}/y_{DM}).

By inserting literature values for Mo, Sr, and Nd concentrations and isotope compositions from the literature (Table S-2) into above equations, this leads to two unknowns of the sediment endmember, a_{SED} and y_{SED}. By varying $a_{SED-MIN}$ to $a_{SED-MAX}$ and $y_{SED-MIN}$ to $y_{SED-MAX}$, a total least squares error can be determined for each $\delta^{98/95}Mo^{exp}$ generated at a given ${}^{87}Sr/{}^{86}Sr$ or ${}^{143}Nd/{}^{144}Nd$ against the observed sample points

$$\sum_{i=a_{SED-min}}^{a_{SED-max}} \sum_{j=y_{SED-min}}^{y_{SED-max}} \sqrt{\left(\delta^{98/95}Mo_{i,j}^{exp} - \delta^{98/95}Mo^{sample}\right)^2} \quad \text{(S-7)}$$

where $a_{SED-MIN}$ = 0.1 µg/g, $a_{SED-MAX}$ = 100 µg/g, $y_{SED-MIN}$ = -1 ‰, and $y_{SED-MAX}$ = 1 ‰.

In the obtained misfit plot (Fig. 2), the best agreement between potential sediment endmember and measured samples is given by the least squares error (blue) of the misfit function. The white dashed line indicates the sample amount multiplied by the external 2SD reproducibility to obtain a conservative upper limit of model compositions. The white solid line indicates the contour line of the least squares error obtained (see error bar in Fig. 2a+b) added by $\Delta^{98/95}$Mo ≈ 0.1 ‰. For comparison, the compositions of OM-rich sediments sorted by

age intervals (Ye *et al.*, 2021; Table S-2), UCC (Freymuth et al., 2015; Greaney et al., 2020; Rudnick and Gao, 2014; Voegelin et al., 2014; Willbold and Elliott, 2017; Yang et al., 2017), MORB (Bezard et al., 2016; Chen et al., 2021; Gale et al., 2013), pelagic Mn-rich and clastic metasediments (Ahmad et al., 2021), and blueschists and MORB-type eclogites (Ahmad et al., 2021; Chen et al., 2019) are plotted (Fig. 2).

Additional scenarios considered for misfit calculations, such as 1 Ga and 2 Ga model sediments, are plotted in Fig S-3 and show least squares errors similar to Fig. 2. This indicates that a Mid-Proterozoic UCC-like sediment with minor authigenic Mo enrichment is a likely sediment endmember (see main text).

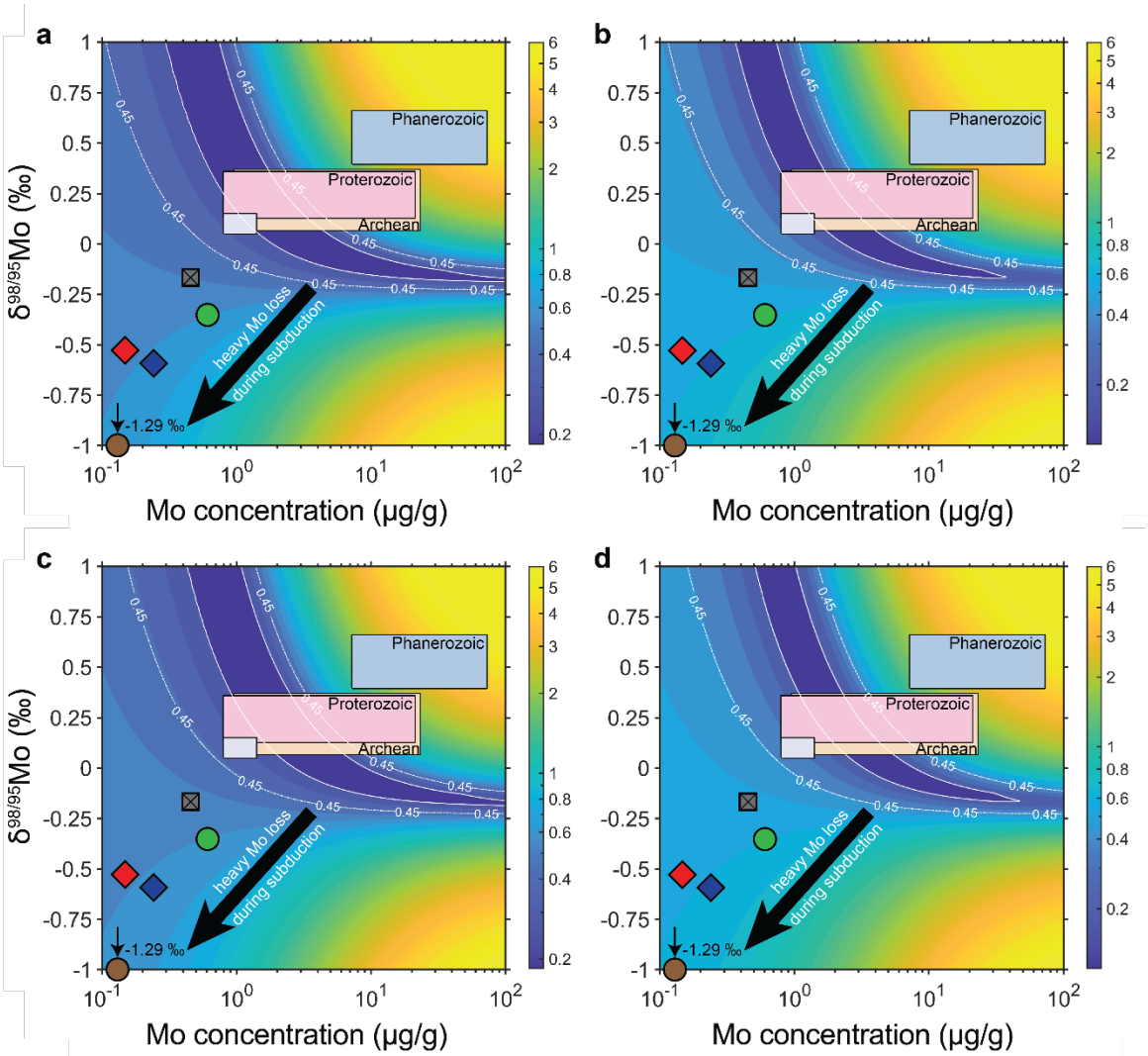

Figure S-3. Misfit calculation based on mixing parameters reported in Fig. 2 and adjusted time-integrated Sr- and Nd isotope composition of the model sediment : a) $^{87}Sr/^{86}Sr$ (1 Ga) = 0.7173; b) $^{143}Nd/^{144}Nd$ (1 Ga) = 0.5115; c) $^{87}Sr/^{86}Sr$ (2 Ga) = 0.7233; d) $^{143}Nd/^{144}Nd$ (2 Ga) = 0.5119.

Table S-2 Parameters from the two-component mixing model (Fig. 2) and compositions of marine sediments.

	$\delta^{98/95}$Mo (‰)	[Mo] (µg/g)	$^{87}Sr/^{86}Sr$	Sr (µg/g)	$^{143}Nd/^{144}Nd$	Nd (µg/g)
End-members						
Ambient depleted mantle	-0.245 ± 0.05[A]	0.025 ± 0.007	0.70250 or *0.702488 ± 0.000032*	9.80 ± 1.86	0.51312 or *0.513135 ± 0.00002*	0.713 ± 0.05
1.5 Ga old recycled pelagic sediment	0.78 ± 0.20[B] or *0.12 ± 0.06*[B]	0.76[B] or *2.98*[B]	0.7203	300 ± 17	0.5117	85 ± 5.2[C]
Marine sediments[D]						
Archean	0.218 ± 0.150 (M=19, N =417)	$4.70^{+18.4}_{-3.75}$ (M=19, N =744)				
Proterozoic	0.244 ± 0.114 (M=51, N =696)	$4.10^{+17.0}_{-3.30}$ (M=53, N =1262)				
Phanerozoic	0.528 ± 0.132 (M=48, N =882)	$22.9^{+49.7}_{-15.7}$ (M=48, N =1154)				

The mixing trends are generated using compositions of the Pacific/ambient depleted mantle or the most depleted MORB: PAC2 DR33-1 & PAC1 CV-02g (in italics). Uncertainties on mixing endmember elemental concentrations (Labidi et al., 2013; Plank, 2014; Rehkämper and Hofmann, 1997; Salters and Stracke, 2004; Yierpan et al., 2020) and on [Mo]-$\delta^{98/95}$Mo values of the marine sediment compilation (Ye et al., 2021) are all 1s (except [Mo] uncertainty in depleted mantle, see Salters and Stracke, 2004).

Pelagic sediment and ambient mantle endmember isotope composition (Andres et al., 2002; Labidi et al., 2014; le Roux et al., 2002c; Rehkämper and Hofmann, 1997; Yierpan et al., 2020) are reported with 1s uncertainties, (except $\delta^{98/95}$Mo uncertainty, which is reported as 2s). *M* = number of age-averaged data, *N* = number of different sediment samples from the literature.

[A] The Mo isotope composition of the Pacific-Antarctic Ridge (PAR) basalts can be used as the depleted mantle endmember, because their Sr and Nd isotope composition match the S-MAR ambient depleted mantle isotopic composition determined previously (Andres et al., 2002; Douglass et al., 1999). The Mo isotope composition of the depleted N-MORB DR33-1g ($\delta^{98/95}$Mo = -0.245 ± 0.05 ‰) matches the light isotope composition of Phanerozoic Gorgona komatiites ($\delta^{98/95}$Mo = -0.18 to -0.25 ‰, McCoy-West *et al.*, 2019) and the lighter end of PAR basalts measured previously ($^{98/95}$Mo = -0.06 to -0.24 ‰, excluding the three heavy outliers; Bezard *et al.*, 2016). Because $\delta^{98/95}$Mo values of S-MAR basalts (and MORBs from EPR and PAR, Fig. 1) extend towards slightly lower values (but still within error) compared to the mean depleted mantle estimate (*e.g.*, McCoy-West *et al.*, 2019), we use this lower end of observed literature values for the ambient depleted mantle. The depleted N-MORB CV-02g ($\delta^{98/95}$Mo = -0.297 ± 0.05 ‰), however, represents an outlier being lighter than this range (but still within error) and is excluded in this model.

[B] Obtained best-fit parameters from linear correlation between Mo-Sr isotope and Mo-Nd isotope (italic font) trend and the Mo, Sr, and Nd contents of depleted mantle and 1.5 Ga pelagic sediment (see above). Note the discrepancy between both $\delta^{98/95}$Mo and [Mo] obtained from both relationships (Fig. 1).

[C] Assigned relative error from GLOSS-II (Plank, 2014) as there was no uncertainty considered for pelagic sediment Nd content.

[D] Marine sediment values of different eons are log-normal means of sediments sorted by age intervals (> 1 Myr) from the literature (see compilation of Ye *et al.*, 2021).

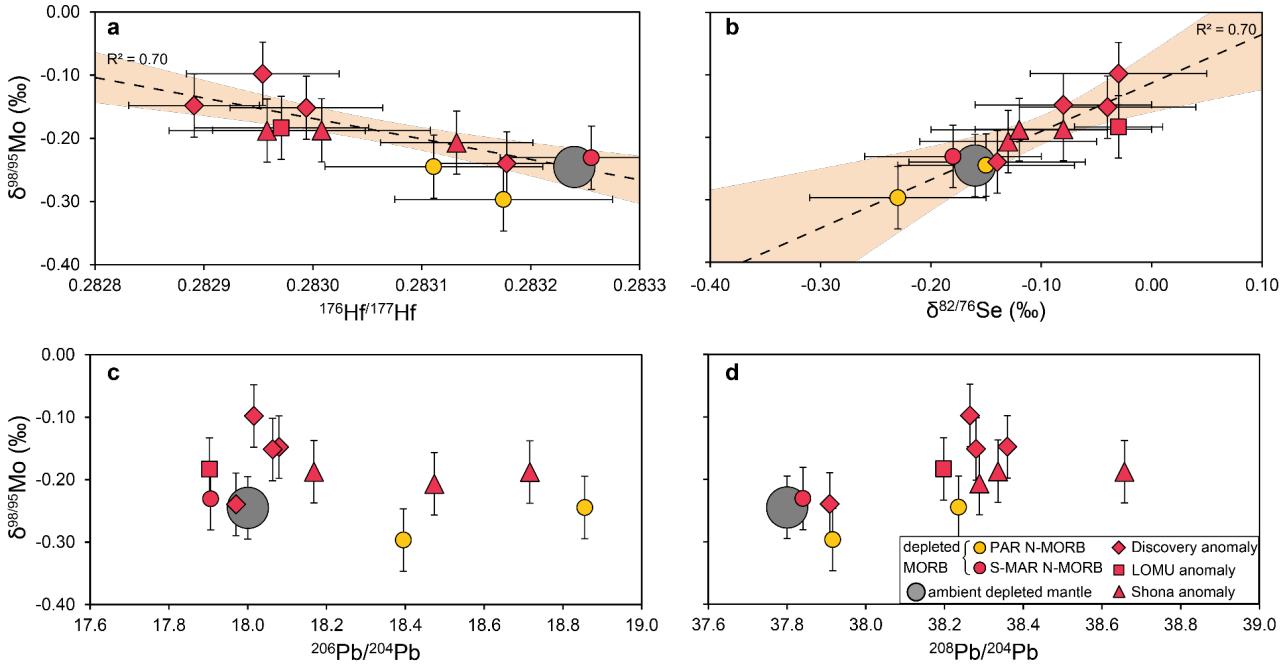

Figure S-4: Covariation diagram of S-MAR samples with: (a) $\delta^{98/95}$Mo vs. ^{176}Hf/^{177}Hf; (b) $\delta^{98/95}$Mo vs. δ^{82}Se (c) $\delta^{98/95}$Mo vs. ^{206}Pb/^{204}Pb; (d) $\delta^{98/95}$Mo vs. ^{208}Pb/^{204}Pb. Error bars indicate 2SD standard deviation external reproducibility. External reproducibility on each isotope value is considered for regression in (a) and (b), and shaded area indicates 95% CI error envelope. PAR samples are excluded from the regression. Radiogenic isotopes, and Se isotopes for this sample set together with ambient depleted mantle values are from (Andres et al., 2002; Douglass et al., 1999; Yierpan et al., 2020).

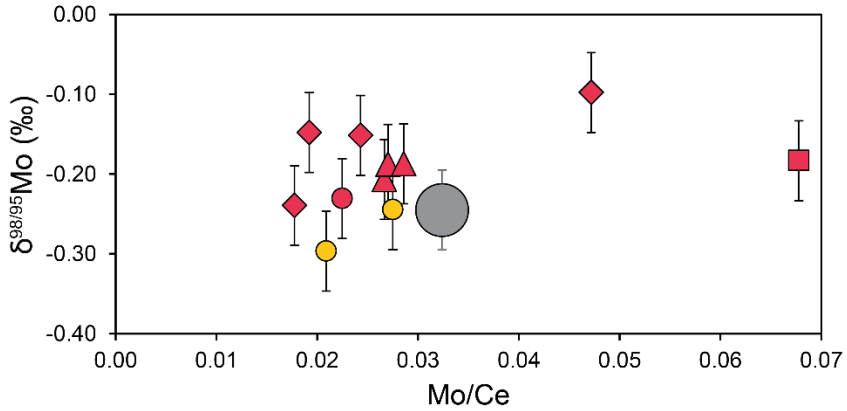

Figure S-5: Covariation diagram of S-MAR samples with $\delta^{98/95}$Mo vs. Mo/Ce. Ce contents of samples and depleted mantle Mo/Ce are from (Kelley et al., 2013; Salters & Stracke, 2004).

Supplementary Information References

Ahmad, Q., Wille, M., König, S., Rosca, C., Hensel, A., Pettke, T., Hermann, J., 2021. The Molybdenum isotope subduction recycling conundrum: A case study from the Tongan subduction zone, Western Alps and Alpine Corsica. Chem. Geol. 576, 120231. https://doi.org/10.1016/J.CHEMGEO.2021.120231

Andres, M., Blichert-Toft, J., Schilling, J.-G., 2002. Hafnium isotopes in basalts from the southern Mid-Atlantic Ridge from 40°S to 55°S: Discovery and Shona plume–ridge interactions and the role of recycled sediments. Geochemistry, Geophys. Geosystems 3, 1–25. https://doi.org/10.1029/2002GC000324

Bezard, R., Fischer-Gödde, M., Hamelin, C., Brennecka, G.A., Kleine, T., 2016. The effects of magmatic processes and crustal recycling on the molybdenum stable isotopic composition of Mid-Ocean Ridge Basalts. Earth Planet. Sci. Lett. 453, 171–181. https://doi.org/10.1016/j.epsl.2016.07.056

Burkhardt, C., Hin, R.C., Kleine, T., Bourdon, B., 2014. Evidence for Mo isotope fractionation in the solar nebula and during planetary differentiation. Earth Planet. Sci. Lett. 391, 201–211. https://doi.org/10.1016/j.epsl.2014.01.037

Chen, S., Hin, R.C., John, T., Brooker, R., Bryan, B., Niu, Y., Elliott, T., 2019. Molybdenum systematics of subducted crust record reactive fluid flow from underlying slab serpentine dehydration. Nat. Commun. 10. https://doi.org/10.1038/s41467-019-12696-3

Chen, S., Sun, P., Niu, Y., Guo, P., Elliott, T., Hin, R.C., 2022. Molybdenum isotope systematics of lavas from the East Pacific Rise: Constraints on the source of enriched mid-ocean ridge basalt. Earth Planet. Sci. Lett. 117283. https://doi.org/10.1016/J.EPSL.2021.117283

Douglass, J., Schilling, J.-G., Fontignie, D., 1999. Plume-ridge interactions of the Discovery and Shona mantle plumes with the southern Mid-Atlantic Ridge (40°-55°S). J. Geophys. Res. Solid Earth 104, 2941–2962. https://doi.org/10.1029/98JB02642

Douglass, J., Schilling, J. -G, Kingsley, R.H., Small, C., 1995. Influence of the discovery and Shona mantle plumes on the southern Mid-Atlantic Ridge: Rare earth evidence. Geophys. Res. Lett. 22, 2893–2896. https://doi.org/10.1029/95GL02665

Freymuth, H., Vils, F., Willbold, M., Taylor, R.N., Elliott, T., 2015. Molybdenum mobility and isotopic fractionation during subduction at the Mariana arc. Earth Planet. Sci. Lett. 432, 176–186. https://doi.org/10.1016/j.epsl.2015.10.006

Gale, A., Dalton, C.A., Langmuir, C.H., Su, Y., Schilling, J.G., 2013. The mean composition of ocean ridge basalts. Geochemistry, Geophys. Geosystems 14, 489–518. https://doi.org/10.1029/2012GC004334

Goldberg, T., Gordon, G., Izon, G., Archer, C., Pearce, C.R., McManus, J., Anbar, A.D., Rehkämper, M., 2013. Resolution of inter-laboratory discrepancies in Mo isotope data: An intercalibration. J. Anal. At. Spectrom. 28, 724–735. https://doi.org/10.1039/c3ja30375f

Greaney, A.T., Rudnick, R.L., Romaniello, S.J., Johnson, A.C., Gaschnig, R.M., Anbar, A.D., 2020. Molybdenum isotope fractionation in glacial diamictites tracks the onset of oxidative weathering of the continental crust. Earth Planet. Sci. Lett. 534, 116083. https://doi.org/10.1016/J.EPSL.2020.116083

Greber, N.D., Siebert, C., Nägler, T.F., Pettke, T., 2012. δ98/95Mo values and Molybdenum Concentration Data for NIST SRM 610, 612 and 3134: Towards a Common Protocol for Reporting Mo Data. Geostand. Geoanalytical Res. 36, 291–300. https://doi.org/10.1111/j.1751-908X.2012.00160.x

Hamelin, C., Dosso, L., Hanan, B.B., Moreira, M., Kositsky, A.P., Thomas, M.Y., 2011. Geochemical portray of the Pacific Ridge: New isotopic data and statistical techniques. Earth Planet. Sci. Lett. 302, 154–162. https://doi.org/10.1016/J.EPSL.2010.12.007

Kelley, K.A., Kingsley, Richard, Schilling, J.-G., A, K.K., Kingsley, R, Schilling, J., 2013. Composition of plume-influenced mid-ocean ridge lavas and glasses from the Mid-Atlantic Ridge, East Pacific Rise, Galápagos Spreading Center, and Gulf of Aden. Geochemistry, Geophys. Geosystems 14, 223–242. https://doi.org/10.1002/GGGE.20049

Labidi, J., Cartigny, P., Hamelin, C., Moreira, M., Dosso, L., 2014. Sulfur isotope budget (32S, 33S, 34S and 36S) in Pacific–Antarctic ridge basalts: A record of mantle source heterogeneity and hydrothermal sulfide assimilation. Geochim. Cosmochim. Acta 133, 47–67. https://doi.org/10.1016/J.GCA.2014.02.023

Labidi, J., Cartigny, P., Moreira, M., 2013. Non-chondritic sulphur isotope composition of the terrestrial mantle. Nat. 2013 5017466 501, 208–211. https://doi.org/10.1038/nature12490

le Roux, P.J., Le Roex, A., Schilling, J.G., 2002a. Crystallization processes beneath the southern Mid-Atlantic Ridge (40–55°S), evidence for high-pressure initiation of crystallization. Contrib. to Mineral. Petrol. 2001 1425 142, 582–602. https://doi.org/10.1007/S00410-001-0312-Y

le Roux, P.J., le Roex, A.P., Schilling, J.G., 2002b. MORB melting processes beneath the southern Mid-

Atlantic Ridge (40–55°S): a role for mantle plume-derived pyroxenite. Contrib. to Mineral. Petrol. 2002 1442 144, 206–229. https://doi.org/10.1007/S00410-002-0376-3

le Roux, P.J., Le Roex, A.P., Schilling, J.G., Shimizu, N., Perkins, W.W., Pearce, N.J.G., 2002c. Mantle heterogeneity beneath the southern Mid-Atlantic Ridge: trace element evidence for contamination of ambient asthenospheric mantle. Earth Planet. Sci. Lett. 203, 479–498. https://doi.org/10.1016/S0012-821X(02)00832-4

Liang, Y.H., Halliday, A.N., Siebert, C., Fitton, J.G., Burton, K.W., Wang, K.L., Harvey, J., 2017. Molybdenum isotope fractionation in the mantle. Geochim. Cosmochim. Acta 199, 91–111. https://doi.org/10.1016/j.gca.2016.11.023

McCoy-West, A.J., Chowdhury, P., Burton, K.W., Sossi, P., Nowell, G.M., Fitton, J.G., Kerr, A.C., Cawood, P.A., Williams, H.M., 2019. Extensive crustal extraction in Earth's early history inferred from molybdenum isotopes. Nat. Geosci. 12, 946–951. https://doi.org/10.1038/s41561-019-0451-2

Moreira, M., Staudacher, T., Sarda, P., Schilling, J.G., Allègre, C.J., 1995. A primitive plume neon component in MORB: The Shona ridge-anomaly, South Atlantic (51–52°S). Earth Planet. Sci. Lett. 133, 367–377. https://doi.org/10.1016/0012-821X(95)00080-V

Nebel-Jacobsen, Y., Wille, M., Ivanic, T., Nebel, O., 2021. Molybdenum isotope systematics in cumulate rock of the 2.8 Windimurra layered intrusion: A test for igneous differentiation and the composition of the Archean mantle. Precambrian Res. 355, 106087. https://doi.org/10.1016/J.PRECAMRES.2020.106087

Plank, T., 2014. The Chemical Composition of Subducting Sediments. Treatise Geochemistry Second Ed. 4, 607–629. https://doi.org/10.1016/B978-0-08-095975-7.00319-3

Rehkämper, M., Hofmann, A.W., 1997. Recycled ocean crust and sediment in Indian Ocean MORB. Earth Planet. Sci. Lett. 147, 93–106. https://doi.org/10.1016/S0012-821X(97)00009-5

Rudnick, R.L., Gao, S., 2014. Composition of the Continental Crust, in: Treatise on Geochemistry: Second Edition. Elsevier Inc., pp. 1–51. https://doi.org/10.1016/B978-0-08-095975-7.00301-6

Salters, V.J.M., Stracke, A., 2004. Composition of the depleted mantle. Geochemistry, Geophys. Geosystems 5, n/a-n/a. https://doi.org/10.1029/2003GC000597

Sarda, P., Moreira, M., Staudacher, T., Schilling, J.G., Allègre, C.J., 2000. Rare gas systematics on the southernmost Mid-Atlantic Ridge: Constraints on the lower mantle and the Dupal source. J. Geophys. Res. Solid Earth 105, 5973–5996. https://doi.org/10.1029/1999JB900282

Siebert, C., Nägler, T.F., Kramers, J.D., 2001. Determination of molybdenum isotope fractionation by double-spike multicollector inductively coupled plasma mass spectrometry. Geochemistry, Geophys. Geosystems 2. https://doi.org/10.1029/2000GC000124

Stracke, A., 2012. Earth's heterogeneous mantle: A product of convection-driven interaction between crust and mantle. Chem. Geol. 330–331, 274–299. https://doi.org/10.1016/J.CHEMGEO.2012.08.007

Voegelin, A.R., Pettke, T., Greber, N.D., von Niederhäusern, B., Nägler, T.F., 2014. Magma differentiation fractionates Mo isotope ratios: Evidence from the Kos Plateau Tuff (Aegean Arc). Lithos 190–191, 440–448. https://doi.org/10.1016/j.lithos.2013.12.016

Vollmer, R., 1976. Rb-Sr and U-Th-Pb systematics of alkaline rocks: the alkaline rocks from Italy. Geochim. Cosmochim. Acta 40, 283–295. https://doi.org/10.1016/0016-7037(76)90205-2

Wang, Z., Becker, H., 2018. Molybdenum partitioning behavior and content in the depleted mantle: Insights from Balmuccia and Baldissero mantle tectonites (Ivrea Zone, Italian Alps). Chem. Geol. 499, 138–150. https://doi.org/10.1016/j.chemgeo.2018.09.023

Willbold, M., Elliott, T., 2017. Molybdenum isotope variations in magmatic rocks. Chem. Geol. 449, 253–268. https://doi.org/10.1016/j.chemgeo.2016.12.011

Willbold, M., Hibbert, K., Lai, Y.-J., Freymuth, H., Hin, R.C., Coath, C., Vils, F., Elliott, T., 2016. High-Precision Mass-Dependent Molybdenum Isotope Variations in Magmatic Rocks Determined by Double-Spike MC-ICP-MS. Geostand. Geoanalytical Res. 40, 389–403. https://doi.org/10.1111/j.1751-908X.2015.00388.x

Wille, M., Nebel, O., Pettke, T., Vroon, P.Z., König, S., Schoenberg, R., 2018. Molybdenum isotope variations in calc-alkaline lavas from the Banda arc, Indonesia: Assessing the effect of crystal fractionation in creating isotopically heavy continental crust. Chem. Geol. 485, 1–13. https://doi.org/10.1016/j.chemgeo.2018.02.037

Wille, M., Nebel, O., Van Kranendonk, M.J., Schoenberg, R., Kleinhanns, I.C., Ellwood, M.J., 2013. Mo-Cr isotope evidence for a reducing Archean atmosphere in 3.46-2.76Ga black shales from the Pilbara, Western Australia. Chem. Geol. 340, 68–76. https://doi.org/10.1016/j.chemgeo.2012.12.018

Yang, J., Barling, J., Siebert, C., Fietzke, J., Stephens, E., Halliday, A.N., 2017. The molybdenum isotopic

compositions of I-, S- and A-type granitic suites. Geochim. Cosmochim. Acta 205, 168–186. https://doi.org/10.1016/j.gca.2017.01.027

Ye, Y., Zhang, S., Wang, H., Wang, X., Tan, C., Li, M., Wu, C., Canfield, D.E., 2021. Black shale Mo isotope record reveals dynamic ocean redox during the Mesoproterozoic Era. Geochemical Perspect. Lett. 18, 16–21. https://doi.org/10.7185/GEOCHEMLET.2118

Yierpan, A., König, S., Labidi, J., Schoenberg, R., 2020. Recycled selenium in hot spot–influenced lavas records ocean-atmosphere oxygenation. Sci. Adv. 6, eabb6179. https://doi.org/10.1126/SCIADV.ABB6179

Zhao, P.-P., Li, J., Zhang, L., Wang, Z.-B., Kong, D.-X., Ma, J.-L., Wei, G.-J., Xu, J.-F., 2016. Molybdenum Mass Fractions and Isotopic Compositions of International Geological Reference Materials. Geostand. Geoanalytical Res. 40, 217–226. https://doi.org/10.1111/j.1751-908X.2015.00373.x